ARCTIC BIOMASS BURNING AEROSOL EVENT– MICROPHYSICAL PROPERTY RETRIEVAL

Böckmann, Christine[1,*]**, Ritter, Christoph**[2] **and Ortiz-Amezcua, Pablo**[3]

[1]*University of Potsdam, Institute of Mathematics, Germany,* *bockmann@uni-potsdam.de*
[2]*Alfred Wegener Institute for Polar and Marine Research, Germany*
[3]*University of Granada, Department of Applied Physics, Spain*

ABSTRACT

An intense biomass-burning (BB) event from North America in July 2015 was observed over Ny-Ålesund (Spitsbergen, European Arctic). An extreme air pollution took place and aerosol optical depth (AOD) of more than 1 at 500nm occurs in middle and lower troposphere. We analyse data from the multi-wavelength Raman-lidar KARL of Alfred Wegener Institute to derive microphysical properties of the aerosol of one interesting layer from 3186 to 3306 m via regularization. We found credible and confidential microphysical parameters.

1 INTRODUCTION

The data for this work was obtained in Ny-Ålesund, Spitsbergen, in the European Arctic on 10 July 2015. An intensive event of BB aerosol originating from the boreal North America was observed for several days around that period at different Arctic sites (Markowicz et al. [1]) and produced an AOD(500) >1. Profiles of extinction and backscatter were obtained by the "3+2" Raman lidar KARL according to the method of Ansmann [2] with 10min / 30m resolution.

This event of BB aerosol and the KARL lidar are described also in [3]. The extinction and backscatter coefficient profiles are shown in Fig 1. For the inversion of the microphysics we selected an altitude range from 3186m to 3306m because a contemporaneous radiosonde showed a humidity about 80-85% and, hence, we expected a larger effective radius and a lower refractive index (RI) as was reported for dry BB aerosol in literature. Wandinger et al [4] derived for example effective radii of 0.25μm and RI of 1.56–1.66 for the real (Re)

and 0.05i–0.07i for the imaginary part (Im).

2 METHODOLOGY

The model relating the optical parameters $\Gamma(\lambda)$ with the volume size distribution $v(r)$ is described by the action of a Fredholm integral operator of the 1st kind with the kernel function $K(r,\lambda;m) = \frac{3}{4r}Q(r,\lambda;m)$ and

$$\Gamma(\lambda) = \int_{r_{\min}}^{r_{\max}} K(r,\lambda;m)v(r)\mathrm{d}r, \qquad (1)$$

where λ is the wavelength, r is the radius, $r_{\min}$, $r_{\max}$ are suitable lower and upper radius bounds, m is the complex RI, $\Gamma(\lambda)$ denotes either the extinction or backscatter coefficients, and Q stands for either the extinction or the backscatter (dimensionless) Mie efficiencies respectively. The wavelength in our measurement cases can only take three discrete values 355, 532, and 1064 nm, since all the measurements were performed with the Raman lidar forming data sets of 3 backscatter coefficients in all three wavelengths and 2 extinction coefficients in the first two. Identifying $\Gamma(\lambda)$ as our measurement data and $v(r)$ as the unknown volume distribution, the problem reduces to the inversion of Eq. (1). Knowing the volume distribution, we can then extract the following microphysical parameters

• total surface-area concentration (μm^{2}cm^{-3})
$s_\mathrm{t} = 3\int \frac{v(r)}{r}\mathrm{d}r$
• total volume concentration (μm^{3}cm^{-3})
$v_\mathrm{t} = \int v(r)\mathrm{d}r$
• total number concentration (cm^{-3})
$n_\mathrm{t} = 3/4\pi \int \frac{v(r)}{r^3}\mathrm{d}r$
• effective radius (μm) $\quad r_\mathrm{eff} = 3\frac{v_t}{s_t}$.

In addition, the complex RI and the single scattering albedo (SSA) in 355 nm and 532 nm are retrieved. Note, that in this work the com-

Table 1: Retrieved RI and SSA using both methods.

	TSVD best point	TSVD mean	TSVD deviation	ITER
RI Re	1.45	1.48	± 0.02	1.49
RI Im	0.001	0.007	± 0.005	0.01
SSA (355)	0.981	0.919	± 0.030	—
SSA (532)	0.987	0.942	± 0.017	—

mon assumption of wavelength-independent RI is made, as a member of the predefined grid introduced, see e.g. [5, 6, 7]. Solving Eq. (1) requires discretization, regularization and a parameter choice rule, see e.g. [5, 8].

2.1 TSVD regularization

We discretized Eq. (1) with spline collocation. The volume distribution $v(r)$ is approximated with respect to the B-spline functions ϕ_j by $v_n = \sum_{j=1}^{n} b_j \phi_j$, reducing the problem to the determination of the coefficients b_j. The continuous problem (Eq. (1)) is now replaced by a discrete one $Ab = \Gamma$, where the matrix elements of the linear system are

$$A_{ij} = \int_{r_{\min}}^{r_{\max}} K(\lambda_i, r; m) \phi_j(r) \mathrm{d}r \qquad (2)$$

and Γ is a vector now. By doing so, we have already projected our problem to a finite n-dimensional space. Clearly, the decision about the projected dimension (n) and order (d) of the base functions ϕ_j is critical, since an appropriate representation of our solution strongly depends on it. This is not done at once; on the contrary, the algorithm constructs a linear system $(5 \times n)$ for each value of n and d specified and every RI within our predefined grid. For example, we first fix the refractive index, and calculate the kernel functions, then decide for candidates for n and d, e.g., $n = 3, \ldots, 8$ and $d = 3, 4$ which define a B-spline function and finally calculate the matrix elements from Eq. (2). For more particular details on the B-spline basis in the frame of a non-negative size distribution, we are looking for, see [5].

Each linear system is solved by first expanding the matrix using Singular Value Decomposition (SVD). Potential noise in our matrix will be magnified as a result of the singular values clustering to zero. We would like to prevent this behavior by including only a part of the SVD, i.e defining a certain cut-off level k, above which the most noisy solution coefficients are filtered out. This regularization procedure is known as Truncated SVD (TSVD), see [5].The parameter choice rule consists in selecting an appropriate triple (n, d, k) heuristically.

2.2 Iterative regularization

A particular iterative regularization (ITER) was used additionally to retrieve microphysical properties of this event. This method is based on Runge-Kutta regularization, see [8, 9]. Since the noise level of the backscatter and extinction profile is often not known or only a roughly estimation is available, a heuristical parameter choice rule is used here too, the well-known L-curve method. This method was developed to retrieve the fine mode only until 1.25μm.

3 RESULTS

The retrieval by TSVD was first done with a refractive index grid with a resolution of 40x40 points and a range for the Re of RI from 1.3-1.8 and for the Im from 0-0.05. We found that the best possible RI's lay on a diagonal pattern what is an indication of precise measurements in agreement with investigated simulations, see [10]. The best points are situated in the range 1.4-1.55 for Re and 0-0.025 for Im. Therefore, the retrieval was done a second time on those ranges with a grid resolution of 20x20, see Fig. 2 (top). We selected the 12 points with a relative residual norm below 8% and a similar shape of the volume distribution. The best point (7.22%) was found for $m = 1.45 + 0.00132i$. Averaging all 12 selected RI points results in $m = 1.48 + 0.00713i$, see Table 1. Additionally, the second algorithm ITER found a similar value $m = 1.49 + 0.01i$ which is in accor-
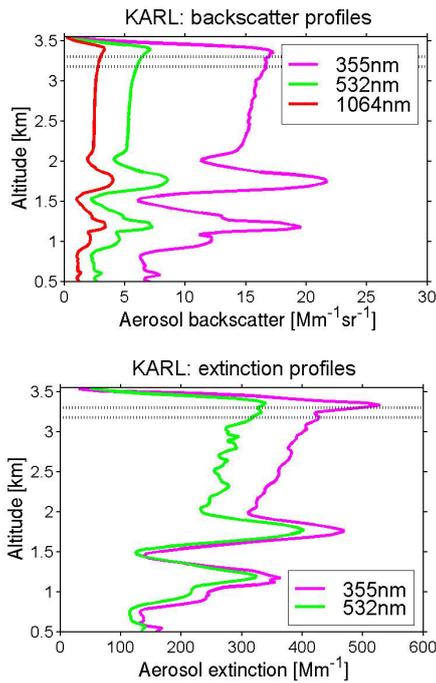
Figure 1: Optical backscatter and extinction coefficient profiles from Raman lidar KARL and aerosol layer of interest (dotted horizontal lines).
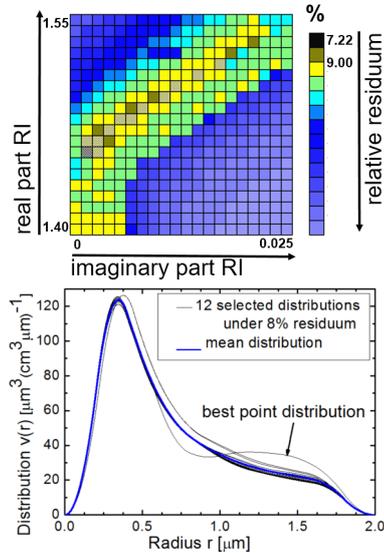
Figure 2: Top: Retrieved complex refractive index grid. Bottom: 12 retrieved volume distributions (thin black lines) and mean distribution (thick blue line).

dance with the deviation level from the first algorithm, see Table 1. Comparing both algorithms for the used B-spline bases yields: Both
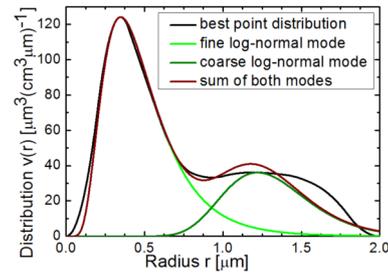
Figure 3: Retrieved volume distribution of the best point, see Fig. 2 with TSVD and two log-normal modes for fine and coarse mode (green lines).

Table 2: Retrieved microphysical properties of the inverted and fitted distributions. Values in brackets stand for: (.) best point and {.} used r_{min}=0.125 µm (regular used r_{min}=0.001 µm).

	mean TSVD	fine mode	coarse mode
r_{med}	—	0.19 (0.22)	1.60 (1.11)
σ	—	1.71 (1.63)	1.08 (1.24)
r_{eff}	0.45 ±0.01 (0.46)	0.40 —— (0.39)	1.63 —— (1.24)
v_t	83.7 ±2.24 (87.0)	66.3 —— (59.2)	6.1 ——- (24.02)
s_t	561 ±2.5 (564)	501 —— (454)	11.25 —— (58.2)
n_t	{477} ({479})	602 (478)	0.35 (3.5)

determined for all selected distributions $n = 8$ (only two outliers $n = 7, 9$) and $d = 3$ for the number and degree of the used splines, respectively. Moreover, with respect to TSVD no additional cut of any singular value was necessary. The retrieved mean volume distribution, see Fig. 2 bottom (blue line), and in particular the best point distribution shows obviously a bi-modal volume distribution, one for the fine mode and one for the coarse mode particles. It is commonly assumed that the number distribution is a log-normal distribution, this property is also true for the surface-area and the volume

distribution with the same geometric standard deviation as well. Therefore, we separated the distribution into two modes by using two log-normal distributions such that the sum of both modes (brown line) fits the retrieved volume distribution well, see Fig. 3. Finally, we summarized all microphysical parameters in Table 2 for the whole distribution as well as for the two modes separately. We remark, that for the total number concentration of the complete mean distribution the Aitken-mode (first part of the fine mode) was excluded since even very small uncertainties in the volume distribution by dividing by r^3 with very small radii lead to a huge amplification.

4 CONCLUSIONS

We found for the effective radius of the complete mean distribution $r_{\text{eff}} = 0.45 \pm 0.01 \mu\text{m}$ as well as for the fine and coarse mode $0.40 \mu\text{m}$ and $1.24 \mu\text{m}$, respectively. Our expectation was approved. Because of the large humidity 80-85% in the regarded particle layer, the effective radius of the BB-particles is larger as usual in the literature, e.g. $0.25 \mu\text{m}$ in [4]. Furthermore, in agreement the RI is indeed lower in both parts for such wet particles, compare the Introduction last part and Table 1. Analyzing the whole profile is an ongoing work but some of the particle properties between 2km and 3.3km altitude are also discussed in [3].

ACKNOWLEDGEMENTS

References

[1] Markowicz, K.M., Pakszys, P., Ritter, C., Zielinski, T., Udisti, R., Cappelletti, D., Mazzola, M., Shiobara, M., Lynch, P., Zawadzka, O., Lisok, J., Petelski, T., Makuch, P., Karasinski, G.: 2016, Impact of North American intensive fires on aerosol optical properties measured over the European Arctic in July 2015, accepted at JGR, doi: 10.1002/2016JD025310.

[2] Ansmann, A., Wandinger, U., Riebesell, M., Weitkamp, C., and Michaelis, W. 1992: Independent measurement of extinction and backscatter profiles in cirrus clouds by using a combined Raman elastic-backscatter lidar, Appl. Opt. 31, 7113-7113.

[3] Ritter, C. and Böckmann, C.: Observation of an intensive Biomass Burning Event over Spitsbergen (this issue).

[4] Wandinger, U., Müller, D., Böckmann, C., Althausen, D., Matthias, V., Bösenberg, J., ... and Ansmann, A. (2002). Special Section: Lindenberg Aerosol Chracterization Experiments (LACE): LAC 7 Optical and microphysical characterization of biomass-burning and industrial-pollution aerosols from multiwavelength lidar. Journal of Geophysical Research-Part D-Atmospheres, 107(21), doi: 10.1029/2000JD000202.

[5] Böckmann, C., 2001: Hybrid regularization method for the ill-posed inversion of multiwavelength lidar data to determine aerosol size distributions, *Appl. Opt.* **40**, 1329–1342.

[6] Kirsche, A., 2003: Entwicklung der Runge-Kutta Iteration und Anwendung als Regularisierungsverfahren, *Diploma thesis University of Potsdam*.

[7] Samaras, S., Nicolae, D., Böckmann, C., Vasilescu, J., Binietoglou, J., Labzovskii, L., Toanca, F., and Papayannis, A., 2015: Using Raman-lidar-based regularized microphysical retrievals and Aerosol Mass Spectrometer measurements for the characterization of biomass burning aerosols, *J. Comput. Phys.* **299**, 156–174.

[8] Böckmann, C. and Kirsche, A., 2006: Iterative regularization method for lidar remote sensing, *Comput. Phys. Commun.* **174**, 607–615.

[9] Osterloh, L., Pérez, C., Böhme, D., Baldasano, J. M., Böckmann, C., Schneidenbach, L., and Vicente, D., 2009: Parallel software for retrieval of aerosol distribution from LIDAR data in the framework of EARLINET-ASOS, *Comput. Phys. Commun.* **180**, 2095–2102.

[10] Müller, D., Böckmann, C., Kolgotin, A., Schneidenbach, L., Chemyakin, E., Rosemann, J., Znak, P., and Romanov, A., 2016: Microphysical particle properties derived from inversion algorithms developed in the framework of EARLINET, *Atmos. Meas. Tech.* **9**, 5007–5035.